THE JOURNAL OF PHYSICAL CHEMISTRY A

Article

pubs.acs.org/JPCA

Photoproduct Channels from $BrCD_2CD_2OH$ at 193 nm and the HDO + Vinyl Products from the CD_2CD_2OH Radical Intermediate

Caroline C. Womack,[†] Britni J. Ratliff,[†] Laurie J. Butler,*[,†] Shih-Huang Lee,[‡] and Jim Jr-Min Lin[§]

[†]The James Franck Institute and the Department of Chemistry, University of Chicago, Chicago, Illinois 60637, United States

[‡]National Synchrotron Radiation Research Center, Hsinchu 30076, Taiwan, Republic of China

[§]Institute of Atomic and Molecular Sciences, Academia Sinica, Taipei 10617, Taiwan, Republic of China

Supporting Information

ABSTRACT: We present the results of our product branching studies of the OH + C_2D_4 reaction, beginning at the CD_2CD_2OH radical intermediate of the reaction, which is generated by the photodissociation of the precursor molecule $BrCD_2CD_2OH$ at 193 nm. Using a crossed laser-molecular beam scattering apparatus with tunable photoionization detection, and a velocity map imaging apparatus with VUV photoionization, we detect the products of the major primary photodissociation channel (Br and CD_2CD_2OH), and of the secondary dissociation of vibrationally excited CD_2CD_2OH radicals (OH, C_2D_4/CD_2O, C_2D_3, CD_2H, and CD_2CDOH). We also characterize two additional photodissociation channels, which generate HBr + CD_2CD_2O and DBr + CD_2CDOH, and measure the branching ratio between the C−Br bond fission, HBr elimination, and DBr elimination primary photodissociation channels as 0.99:0.0064:0.0046. The velocity distribution of the signal at m/e = 30 upon 10.5 eV photoionization allows us to identify the signal from the vinyl (C_2D_3) product, assigned to a frustrated dissociation toward OH + ethene followed by D-atom abstraction. The relative amount of vinyl and Br atom signal shows the quantum yield of this HDO + C_2D_3 product channel is reduced by a factor of 0.77 ± 0.33 from that measured for the undeuterated system. However, because the vibrational energy distribution of the deuterated radicals is lower than that of the undeuterated radicals, the observed reduction in the water + vinyl product quantum yield likely reflects the smaller fraction of radicals that dissociate in the deuterated system, not the effect of quantum tunneling. We compare these results to predictions from statistical transition state theory and prior classical trajectory calculations on the OH + ethene potential energy surface that evidenced a roaming channel to produce water + vinyl products and consider how the branching to the water + vinyl channel might be sensitive to the angular momentum of the β-hydroxyethyl radicals.

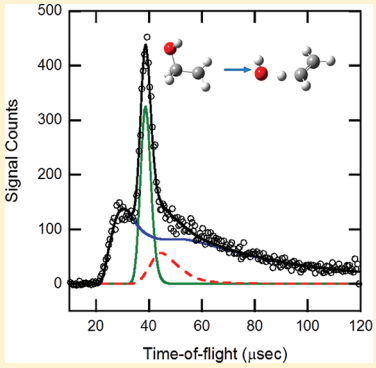

I. INTRODUCTION

Because of the importance of the OH-initiated oxidation of alkenes in combustion and atmospheric chemistry, the study of the reaction of OH + ethene has been the focus of a great number of experimental[1−21] and theoretical[22−28] studies. Many bulk kinetics studies have aimed to elucidate the overall branching of the OH + C_2H_4 reaction, and found that a hydrogen abstraction mechanism dominates at high temperatures, forming H_2O + C_2H_3.[1] At lower temperatures however, the addition of the OH radical to the double bond to form the CH_2CH_2OH radical adduct dominates the kinetics.[22] The overall branching of the OH + C_2H_4 reaction to its various products is dependent on the subsequent dynamics of this radical adduct. Recent studies, both theoretical and experimental, have attempted to determine branching ratios of the product channels of the reaction, beginning at the CH_2CH_2OH (β-hydroxyethyl) radical adduct.[23,29,30]

The CH_2CH_2OH radical intermediate may be produced from the photodissociation of 2-haloethanols. Hintsa et al.[31] were the first to investigate the photodissociation of 2-bromoethanol at 193 nm, showing that a large fraction of β-hydroxyethyl radicals were formed stable to subsequent dissociation to OH + ethene and attributing it to a large partitioning of energy into rotational energy of the radicals. In our previous studies of the OH + C_2H_4 system,[29,32] we generated CH_2CH_2OH radicals via the photodissociation of 2-bromoethanol, and experimentally characterized the product branching. While many of the radicals did not dissociate because much of the energy was partitioned to relative kinetic energy or to rotational rather than vibrational energy, the CH_2CH_2OH radicals that did dissociate evidenced branching fractions of 0.765:0.145:0.026:0.063:<0.01 to the OH + C_2H_4, H_2O + C_2H_3, CH_2CHOH + H, H_2CO + CH_3, and CH_3CHO + H products channels, respectively. One unexpected result was the prevalence of the H_2O + C_2H_3 channel. While this vinyl channel is the dominant product channel in bulk kinetic studies of the OH + C_2H_4 reaction at high temperature and low pressure, we began the dynamics in our study not at this

Special Issue: A. R. Ravishankara Festschrift

Received: December 16, 2011
Revised: March 29, 2012

   dx.doi.org/10.1021/jp212167t | J. Phys. Chem. A XXXX, XXX, XXX−XXX

entrance channel, but at the first radical adduct, CH_2CH_2OH, and conducted the experiments under collision free conditions. Prior statistical transition state predictions[23,29] for the OH + ethene reaction had attributed the vinyl + H_2O product branching to the direct abstraction channel because the transition state from the radical intermediate to H_2O + vinyl was calculated to be much higher in energy. We proposed that the dissociation of the radical to H_2O + C_2H_3 observed in our experiments might involve a frustrated dissociation of the C−O bond toward the $[CH_2CH_2]\cdots$ OH exit channel followed by an H atom abstraction by the OH moiety instead of returning to the CH_2CH_2OH well. In classical trajectory calculations on the global potential energy surface for this reaction, Kamarchik et al.[30] observed a roaming mechanism for the H_2O + vinyl product channel beginning from the radical intermediate. However, their calculations at 44 kcal/mol predicted a smaller branching to these products than was observed experimentally. In an effort to confirm the assignment of this signal to the water + vinyl product channel, and to assess the role of tunneling in the dynamics, we began a comprehensive study of the reaction of OH and deuterated ethene from the CD_2CD_2OH radical intermediate.[33] As in the prior work of Edwards et al.,[34] we produced this radical from the photodissociation of $BrCD_2CD_2OH$.

In our first study,[33] we generated the partially deuterated radical adduct of the OH + C_2D_4 reaction, CD_2CD_2OH, via the photodissociation of 2-bromoethanol-d_4 ($BrCD_2CD_2OH$) and characterized the vibrational energy distribution of the resulting radicals. Using a velocity map imaging apparatus, we characterized the distribution of translational energies, $P(E_T)$, imparted to the Br and CD_2CD_2OH fragments upon C−Br bond fission. Using conservation of energy and a recently proposed model to estimate partitioning of available energy into rotational and vibrational degrees of freedom, we derived from the measured $P(E_T)$ a $P(E_{vib})$ of nascent CD_2CD_2OH radicals, which peaked at 19.5 kcal/mol and spanned nearly 60 kcal/mol. This distribution is shown superimposed on the calculated stationary points on the potential energy surface (PES) of this reaction in the lower frame of Figure 1, reproduced from ref 33. While nearly 80% of the CD_2CD_2OH radicals are formed with vibrational energy below the OH + ethene asymptote and only a very small fraction have enough energy to surmount the abstraction barrier to the HDO + vinyl product channel, these radicals might access the vinyl product channel if tunneling were important in the product branching or if the moment of inertia of the radical changes substantially as it nears the abstraction transition state. We thus undertook the present experiments to investigate whether the branching observed to the water + vinyl product channel from the β-hydroxyethyl radical intermediate might be substantially influenced by these effects.

The available channels for the CD_2CD_2OH radical are shown in Figure 1 and are listed in eqs 1a−1e:

$$CD_2CD_2OH \rightarrow OH + C_2D_4 \qquad \Delta H = 26.3 \text{ kcal/mol} \qquad (1a)$$

$$CD_2CD_2OH \rightarrow HDO + C_2D_3 \qquad \Delta H = 18.4 \text{ kcal/mol} \qquad (1b)$$

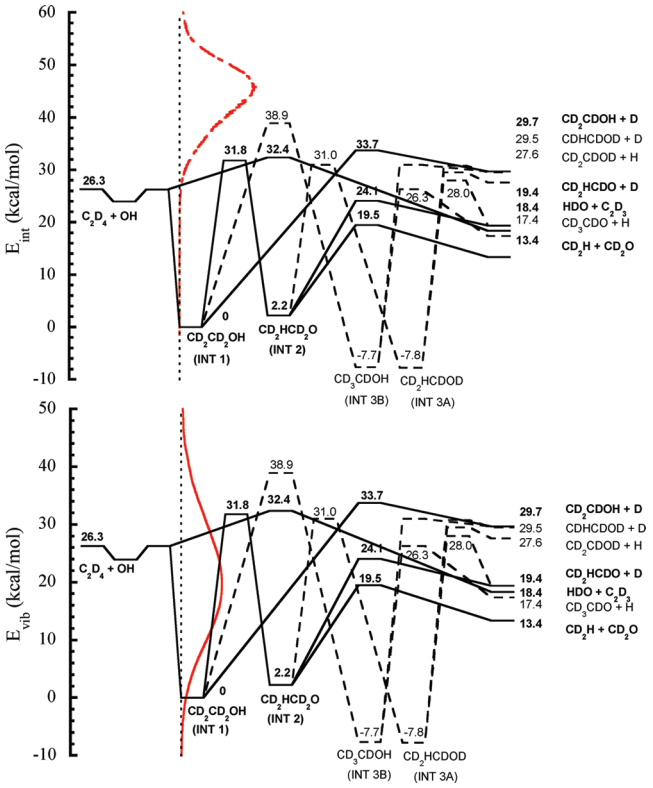

Figure 1. Stationary points on the potential energy surface of the OH + C_2D_4 reaction, calculated at the G4//B3LYP/6-311++G(3df,2p) level of theory, reprinted from Figure 1 of ref 33 . Solid black lines indicate pathways previously calculated by Edwards et al. in ref 34, and dashed lines indicate additional pathways calculated in our previous study. In the upper frame, the distribution of internal energies, E_{vib} + E_{rot}, partitioned to the CD_2CD_2OH radicals is shown in dashed red line. The estimated distribution of vibrational energies partitioned to the nascent CD_2CD_2OH radicals is shown in red solid line in the bottom frame. The internal energy distribution in the top frame is derived from our Br atom TOF distribution using eq 2 in our previous paper, while the vibrational energy distribution in the lower frame is derived from the model therein.[33]

$$CD_2CD_2OH \rightarrow CD_2H + CD_2O \qquad \Delta H = 13.4 \text{ kcal/mol} \qquad (1c)$$

$$CD_2CD_2OH \rightarrow \text{ethenol} + H/D \qquad \Delta H = 27.6 - 29.7 \text{ kcal/mol} \qquad (1d)$$

$$CD_2CD_2OH \rightarrow \text{acetaldehyde} + H/D \qquad \Delta H = 17.4 \text{ or } 19.4 \text{ kcal/mol} \qquad (1e)$$

This work determines the relative branching to the HDO + vinyl product channel of the CD_2CD_2OH radical adduct (eq 1b) using a crossed laser-molecular beam apparatus and a velocity map imaging apparatus, and compares the results to those obtained for the undeuterated system. We find that the vinyl channel is again prevalent in much higher abundance than would be expected by RRKM theory, and the signal again evidences an angular distribution expected for the dissociation of rotationally excited radical intermediates. While the total quantum yield of the water + vinyl channel in the CD_2CD_2OH system is smaller than that in the CH_2CH_2OH system, this reduction is accounted for by the larger fraction of radicals

dx.doi.org/10.1021/jp212167t | J. Phys. Chem. A XXXX, XXX, XXX−XXX

produced stable to subsequent dissociation in the deuterated system. We thus consider the role of angular momentum in the product branching. We also present data on several other product pathways accessed in the dissociation of CD_2CD_2OH radicals, as well as two additional primary photodissociation pathways of the $BrCD_2CD_2OH$ precursor molecule.

II. EXPERIMENTAL SECTION

The CD_2CD_2OH radical was generated in a range of internal energies via the photodissociation of partially deuterated 2-bromoethanol, $BrCD_2CD_2OH$. The time-of-flight spectra of the momentum-matched Br and CD_2CD_2OH cofragments, as well as several dissociation products of unstable CD_2CD_2OH radicals and two minor additional primary photodissociation channels, were measured in a crossed laser-molecular beam scattering apparatus. To elucidate the relative branching to the water + vinyl channel between this system and the undeuterated system, we took additional data on a velocity map imaging apparatus at m/e = 27 ($C_2H_3^+$) and m/e = 30 ($C_2D_3^+$) formed from unstable CH_2CH_2OH and CD_2CD_2OH radicals, respectively. The crossed laser-molecular beam scattering apparatus relies on a very careful calibration of the parent beam velocity, which must be stabilized over several hours, making it impossible to switch back and forth between samples to get a branching ratio. Velocity map imaging is not sensitive to this beam velocity, and thus this apparatus provides an alternate method for detecting a branching ratio between the two systems.

A. Crossed Laser-Molecular Beam Scattering Apparatus. The scattering data presented in this paper were taken at the National Synchrotron Radiation Research Center (NSRRC) in Hsinchu, Taiwan, using the U9 Chemical Dynamics Beamline and a crossed laser-molecular beam scattering apparatus. This apparatus has been described at length elsewhere;[29,35−38] thus, only a brief description will be provided here. A supersonic beam of $BrCD_2CD_2OH$ molecules was created by seeding the vapor pressure of the liquid sample (Sigma-Aldrich, 98% D atoms, used without further purification) in neon to a concentration of 1.25% and expanding the gaseous mixture through a pulsed Even-Lavie valve into a rotating source chamber. The nozzle was heated to 80 °C to minimize molecular clusters in the beam, and it operated at pulse rate of 80 Hz. The parent molecule has five stable conformers, two with a trans geometry between the OH and Br (denoted as the Tt and Tg conformers), and three with a gauche geometry between the OH and Br (denoted as the Gg, Gg′ and Gt conformers). Assuming a thermal distribution at this nozzle temperature, the molecular beam will have 78% of the parent molecules in the gauche conformations.[33] The 193 nm output of a LPF 200 Lambda Physik Laser Technik laser, propagating perpendicularly to the plane created by the molecular beam and the detector axis was aligned directly into the chamber. There, it intersected the molecular beam, exciting the parent molecule to a repulsive excited state and cleaving the C−Br bond. The beam spot measured 4 mm × 3 mm and the pulses typically had energies of approximately 50 mJ/pulse, or approximately 400 mJ/cm^2. The resulting Br and stable CD_2CD_2OH radicals, as well as any products formed as a result of the secondary dissociation of unstable CD_2CD_2OH radicals, recoil in a range of net velocities. Each net velocity is the vector sum of the recoil velocities (both primary and secondary) and the initial velocity of the $BrCD_2CD_2OH$ in the molecular beam. Those fragments with a net velocity vector pointing into the detector traveled the 10.05 cm to the ionizer region, where they were ionized by the tunable VUV synchrotron radiation. This ionization energy was varied by adjusting the U9 undulator gap. A ∼10 Torr rare gas filter (Xe for 7.36−9.61 eV, Kr for 8.82−12.62 eV, Ar for 13.58−15.34 eV, Ne for 12.62−19.29 eV) was used to filter out higher harmonics of the synchrotron radiation.

The ions were focused and accelerated by high voltage plates into an Extrel 1.2 MHz quadrupole mass spectrometer, where they were filtered by mass and counted by a Daly detector. A multichannel scalar counted the signal, which is proportional to the number of ions, and recorded it as a function of total time-of-flight (TOF). This TOF is the sum of the flight time of the neutral fragments to the ionizer, and the flight time of the ionized fragments to the detector. The latter time is determined by the previously calibrated apparatus ion flight constant of 5.36 μs amu$^{-1/2}$. The m/e = 79 (Br^+) data taken at 10°, 20°, 30°, and 40° were collected in 1 μs bins. The remaining data were collected in 0.5 μs bins, and all time-of-flights were corrected to account for the measured 1.1 μs electronic delay between the laser and the triggering of the multichannel scaler. The TOF spectra are fit using a forward convolution method on an guessed distribution of center-of-mass recoil kinetic energies, $P(E_T)$, iteratively adjusting the $P(E_T)$ until it matches the experimental data.

The initial speed distribution of the molecular beam was determined by lowering a 200 Hz chopper wheel into the chamber, aligning the source chamber to 0° and measuring time-of-flight distributions of the daughter ions formed upon dissociative ionization of the parent molecule in the ionizer. As in our previous study of the 2-bromoethanol system, the velocity distribution was found to have a slow tail not fit by the usual expression $N(v) = v^2\, e^{-((v/\alpha)-S)^2}$. We instead fit the data with two distributions, $N_{fast}(v)$ and $N_{slow}(v)$, and summed them to yield the total number density distribution. This distribution, shown in the Supporting Information, peaks at 7.6 × 10^4 cm/s and has a full width at half-maximum of 29%.

Photoionization efficiency (PIE) curves were taken for the m/e = 47 and m/e = 48 signals by integrating the signal counts at ionization energies ranging from 10.0 to 12.6 eV for m/e = 47 and 7.4 to 12.6 eV for m/e = 48. For photoionization energies below 9.21 eV, the rare filter gas was switched from Kr to Xe. To maintain an accurate curve, 3 overlapping data points were taken at 8.82, 9.21, and 9.61 eV with both the Xe and the Kr filter gas, and the PIE curve taken with the Kr filter gas was scaled by the average of the differences at these three data points.

B. Velocity Map Imaging Apparatus. Additional data was taken on a velocity map imaging apparatus modeled on the design of Eppink and Parker.[39,40] This apparatus has been described extensively elsewhere;[32,33,41,42] a brief description is provided here. A beam of $BrCD_2CD_2OH$ molecules was created by seeding the vapor pressure of the liquid sample maintained at 40 °C in helium to a concentration of 1.2%, and expanding the 500 Torr mixture through a General One Iota Valve pulsed valve, with a nozzle diameter of 0.8 mm heated to 80 °C, into a vacuum chamber, and then skimmed upon entering the main chamber maintained at 10^{-6} Torr. The 193 nm output of a GAM EX10 ArF excimer laser was vertically polarized and focused to a point about 3 cm before the intersection with the molecular beam, cleaving the C−Br bond and generating Br and CD_2CD_2OH cofragments in a range of

dx.doi.org/10.1021/jp212167t | J. Phys. Chem. A XXXX, XXX, XXX−XXX

energies. The beam spot measured approximately 0.5 mm^2 and the laser pulses typically had energies of <1 mJ/pulse or 50 mJ/cm^2. The 355 nm output of a Continuum Surelite I-20 Nd:YAG laser was tripled in a xenon cell, and the resulting 118 nm light photoionized the neutral vinyl fragments formed by the dissociation of β-hydroxyethyl radicals. The Br fragments were detected with [2 + 1] resonance enhanced multiphoton ionization (REMPI), using the frequency-tripled output of a dye laser pumped by the second harmonic of a Continuum Powerlite Nd:YAG laser.

The spherically expanding cloud of ions was accelerated down a grounded time-of-flight tube toward a detector consisting of a chevron MCP coupled to a P20 phosphor screen maintained at 3.3 kV above the potential of the rear plate of the MCP. The cloud of ions was pancaked as it traveled toward the detector, and separated according to mass. A −750 V gate was applied to the front plate of the MCP, timed to coincide with the arrival of the fragments of a certain mass-to-charge ratio.[43] The impact of a colliding ion on the MCP generated an electron cascade, which triggered the illumination of the phosphor screen. A CCD camera recorded the images generated on the phosphor screen. The three-dimensional distribution of velocities was extracted from the two-dimensional image, and integrated over all solid angles to yield a distribution of net recoil speeds for each of the fragments.[44]

C. Computational Methods. To calculate appearance energies for daughter ions, the GAUSSIAN09, version A.02 electronic structure package was utilized.[45] The geometries were optimized at the B3LYP/6-311++G(3df,2p) level of theory and the energies were calculated using the G4//B3LYP/6-311++G(3df,2p) method. The geometries were optimized until they converged to a root-mean-square displacement of 4×10^{-5} and a root-mean-square force of 1×10^{-5} (in atomic units). The appearance energies AE(A^+) were calculated by subtracting the G4 energy of the neutral parent, E(AB), from the sum of the G4 energies of the daughter ion, $E(A^+)$, and its neutral cofragment, E(B). RRKM predictions for the branching ratios were calculated using the Multiwell Program Suite with a 1-D Eckart tunneling approximation.[46−48] The vibrational frequencies and moments of inertia utilized for the RRKM predictions were calculated at the B3LYP/6-311++G(3df,2p) level of theory and scaled by 0.9854.[49] We treated all the normal modes of vibration as harmonic vibrations. As in our previous study,[29] the water + vinyl channel was included in the RRKM predictions by assuming that the HDO + C_2D_3 product channel was connected to INT 1 via the 32.4 kcal/mol transition state that connects OH + C_2D_4 to HDO + C_2D_3. We made this assumption because the only transition state that directly connects the CD_2CD_2OH radicals to the water + vinyl product channel is prohibitively high in energy, so we attempted to provide an ad hoc route from CD_2CD_2OH radicals to these products via the abstraction transition state.

III. RESULTS

We present in Section III.A the time-of-flight spectra of the primary photodissociation products obtained on a scattering apparatus, taken at m/e = 49 ($CD_2CD_2OH^+$), m/e = 79 ($^{79}Br^+$), m/e = 82 ($H^{81}Br^+$), and m/e = 83 ($D^{81}Br^+$). Using conservation of momentum, a distribution of center-of-mass translational energies $P(E_T)$ was determined for all C−Br bond fission events from the TOF spectrum of m/e = 79 (Br^+). As demonstrated previously, a portion of the CD_2CD_2OH radicals were formed with sufficient vibrational energy to dissociate to one of the various pathways on the PES and will not be detected.[33] Thus the $P(E_T)$ derived from detecting stable CD_2CD_2OH radicals at m/e = 49 does not match that of m/e = 79 at low E_T's. The difference between the two distributions represents the unstable CD_2CD_2OH radicals that can subsequently dissociate to one of the pathways. Section III.B details the TOF spectra of these products of the secondary dissociation of unstable CD_2CD_2OH radicals. Data were taken at m/e = 17 (OH^+, CD_2H^+), m/e = 19 (HDO^+), m/e = 30 ($C_2D_3^+$), m/e = 32 ($C_2D_4^+$, CD_2O^+), m/e = 47 (CD_2CDOH^+), and m/e = 48 ($CD_2CD_2O^+$). The branching ratios between select product channels were determined on the scattering apparatus, and the ratio between the quantum yield of the water + vinyl channel in the deuterated and the undeuterated system were determined on the velocity map imaging apparatus and are described in Section III.C.

A. Primary Photodissociation Channels. The absorption of a 193 nm photon excites a transition nominally assigned to the promotion of an electron from a nonbonding orbital of the Br to the σ^* orbital of the C−Br bond.[50] These types of excited states are quite repulsive in the Franck−Condon region,[51] and result in a rapid cleavage of the C−Br bond, generating the radicals of interest. Figure 2 shows the TOF spectrum collected

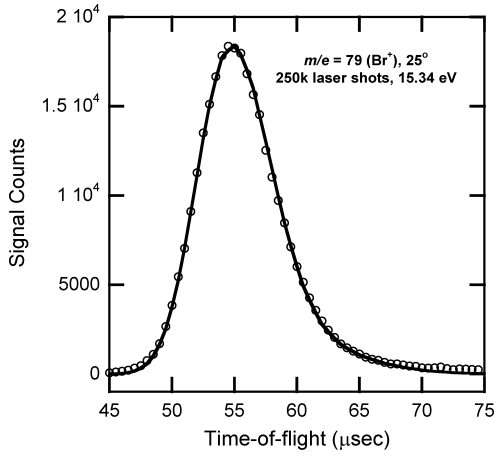

Figure 2. Time-of-flight spectrum of m/e = 79 fragments, attributed to the Br products from C−Br bond fission of the $BrCD_2CD_2OH$ parent molecule. The open circles indicate experimental data, and the black line is the forward convolution fit to the data using the $P(E_T)$ in Figure 3.

at m/e = 79 (Br^+) at a source angle of 25°. The experimental data are shown in black open circles, and are fit using a forward-convolution method. The fit is shown in black solid line, and was derived from the $P(E_T)$ shown in solid black line in Figure 3. This $P(E_T)$ peaks at 34 kcal/mol and spans nearly 30 kcal/mol, which matches fairly well with the $P(E_T)$ previously measured on our velocity map imaging apparatus.[33] The previous $P(E_T)$ also peaks at E_T = 34 kcal/mol but is ∼2 kcal/mol broader on the slow side, likely because of differences in resolution between the two apparatuses. The m/e = 79 data was taken at an ionization energy of 15.34 eV, chosen so that the photoionization cross sections of Br($^2P_{1/2}$) and Br($^2P_{3/2}$) would be equal when corrected for their statistical ratios.[52] In ref 33 it is shown that the spin−orbit selected velocity distributions are similar in this system. Figure 4 shows m/e = 79 data collected at additional source angles of 10°, 20°, 30°, and 40°. Each spectrum was similarly fit using the black solid $P(E_T)$ in

dx.doi.org/10.1021/jp212167t | J. Phys. Chem. A XXXX, XXX, XXX−XXX

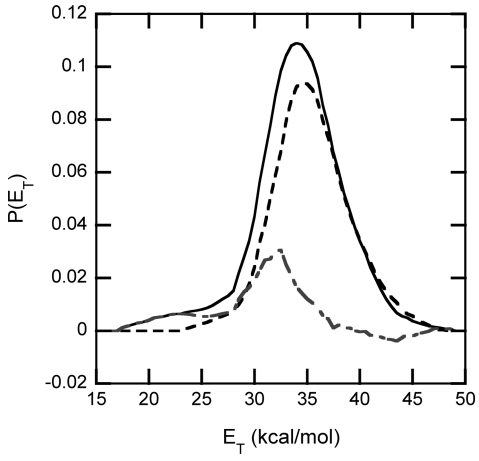

Figure 3. $P(E_T)$s used to fit the m/e = 79 data in Figure 2 (solid) and the m/e = 49 data in Figure 5 (dashed). The two distributions match at high E_T's (i.e., low E_{vib}'s) but diverge at lower E_T's when a portion of the nascent CD_2CD_2OH radicals has sufficient E_{vib} to surmount dissociation barriers. The $P(E_T)$ of unstable radicals, shown in gray dashed-dot line, is obtained by subtracting one $P(E_T)$ from the other.

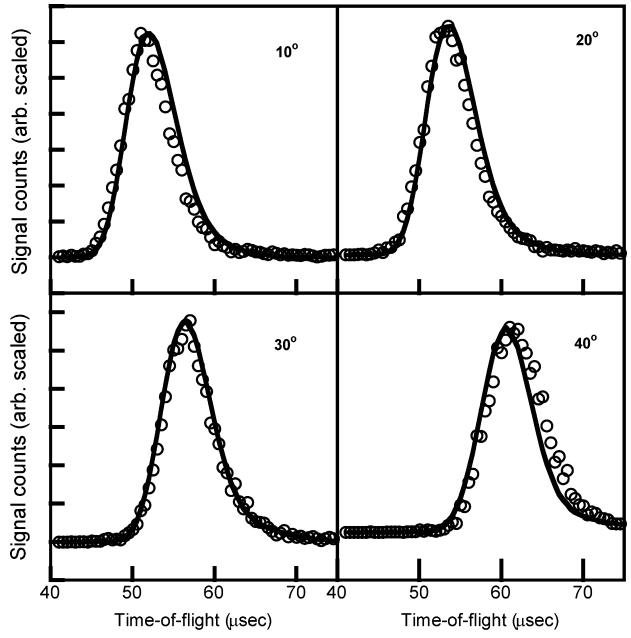

Figure 4. TOF spectra taken at m/e = 79 (Br^+) at source angles of 10°, 20°, 30°, and 40°. The open circles indicate experimental data; the black solid lines are the forward-convolution fits of the $P(E_T)$ shown in black in Figure 3. The signal counts on the y-axis are arbitrarily scaled.

Figure 3. An accurate fit is apparent at 20° and 30°, but the fit is too slow on the 10° data and too fast on the 40° data. This demonstrates that the molecular beam velocity distribution is fairly well characterized, but has a small systematic error. The remaining data were taken at 25°. We can estimate the effect of this small systematic error on the fits of the data taken at 25° for the momentum-matched radicals to the Br atoms. These radicals have a smaller mass and thus a larger recoil velocity in the center-of-mass reference frame. At the tangent to the Newton sphere the Br atoms detected at a source angle of 15° would have momentum-matched cofragments that have a recoil velocity at the tangent to the Newton sphere for data taken at a 25° source angle. Thus the 25° fits at m/e = 49 and similar masses are likely to resemble the smaller angle Br data and the fit should err on the side of being slightly slow.

The cofragment formed in the dominant C−Br fission channel, CD_2CD_2OH, was detected at m/e = 49. Figure 5

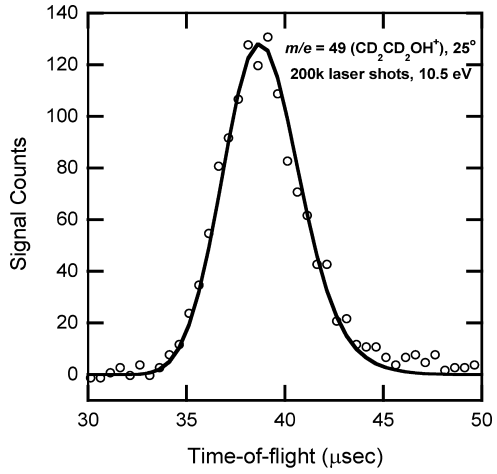

Figure 5. TOF spectrum taken at m/e = 49, attributed to stable CD_2CD_2OH radicals. The open circles indicate experimental data; the forward convolution fit of the $P(E_T)$ shown in black dashed line in Figure 3 is shown here in black solid line.

shows the TOF spectrum of this signal, with the data shown as open circles and the forward-convolution fit shown as a solid line, derived from the $P(E_T)$ in black dashed line in Figure 3. As demonstrated in our previous paper on this system,[33] a portion of the nascent CD_2CD_2OH radicals formed with low translational energy have sufficient vibrational energy to isomerize or dissociate. This result is replicated in the current results, as the $P(E_T)$ used to fit the m/e = 49 data diverges from the $P(E_T)$ used to fit the m/e = 79 data at energies less than 37 kcal/mol. The gray dashed-dot line in Figure 3 shows the calculated $P(E_T)$ of unstable CD_2CD_2OH radicals, obtained by subtracting one $P(E_T)$ from the other. We find by integrating the area under each curve that 80% of the nascent radicals are formed stable to further dissociation, and 20% are unstable and thus may dissociate to one of the various product pathways. The $P(E_T)$ of unstable radicals is used in Section III.B to analyze the velocities measured for the products of the dissociation of these radicals. The velocity imparted to the products in this secondary dissociation is vector summed with the velocity of the unstable radical to obtain the net velocity imparted to the detected secondary products.

In addition to the C−Br fission primary channel, we found evidence of two minor photodissociation channels, the photoelimination of HBr and of DBr. Figure 6 shows the TOF spectra for m/e = 82 ($H^{81}Br^+$) and m/e = 83 ($D^{81}Br^+$) in the top and bottom frame respectively. ^{79}Br and ^{81}Br exist in a nearly 50/50 ratio, and so the detection of HBr and DBr fragments with mass-to-charge ratios of 82 and 83 was preferable to 80 and 81 to avoid the signal from the m/e = 81 ($^{81}Br^+$) signal. The open circles indicate the experimental data, and the black solid lines are the forward convolution fits derived from the $P(E_T)$'s shown in Figure 7. The $P(E_T)$ used to fit the HBr data, shown in solid line in Figure 7, peaks at 38 kcal/mol, which is nearly twice the most probable kinetic energy in the $P(E_T)$ used to fit the DBr data, shown in dashed line. The parent molecule $BrCD_2CD_2OH$ has a single hydrogen

dx.doi.org/10.1021/jp212167t | J. Phys. Chem. A XXXX, XXX, XXX−XXX

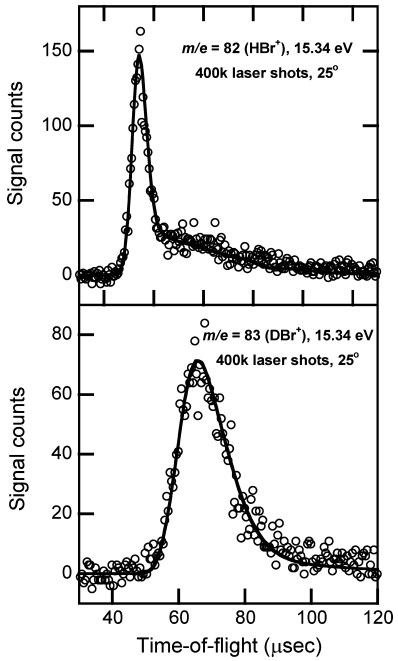

Figure 6. TOF spectra taken at m/e = 82 and m/e = 83, attributed to HBr^+ and DBr^+, respectively. The experimental data is shown in open circles and the black lines are the forward-convoluted fits of the $P(E_T)$'s shown in Figure 7.

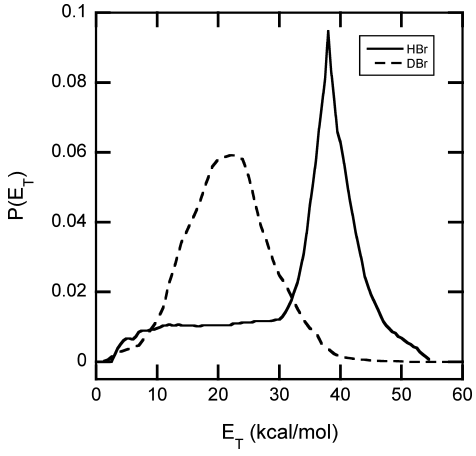

Figure 7. $P(E_T)$'s for the HBr and DBr elimination channels, shown in solid and dashed line respectively, derived from the forward convolution fitting of the spectra in Figure 6.

available to form HBr, the hydroxyl group hydrogen. The elimination to form HBr is thus a 5-center elimination, while the elimination to form DBr must either be a 3- or 4-center elimination. The 4-center elimination likely occurs via internal conversion to the ground electronic state, followed by dissociation of the highly excited molecule over a ~60 kcal/mol barrier to DBr + ethenol. Though the endoergicity is small, such eliminations have been previously shown to partition much of the available energy into vibrational degrees of freedom, leaving significantly less energy to be partitioned to the relative kinetic energy of the two photofragments.[53,54] This trend is evident in our data, as the DBr elimination partitions much less energy to relative kinetic energy compared to the HBr elimination or the C−Br photofission channels. The high relative kinetic energies imparted upon C−Br fission reflect the repulsive forces on the excited electronic state.

The branching ratio between the three primary photodissociation channels is calculated as follows. The relative signal intensities for each fragment are calculated by integrating the fits in Figures 2 and 6 from 20 to 200 μs and dividing by the total number of laser shots. This ratio of signal intensities is corrected by a ratio of expected signal, which takes into account 3-D kinematic scattering factors, Jacobian factors, and transit times through the ionizer. Finally, the ratio is corrected by the ratio of partial photoionization cross sections, which we approximate as 40.0 Mb for HBr^+/HBr and DBr^+/DBr,[55] and 50.4 Mb for Br^+/Br.[52] (In our prior study,[29] we erroneously derived $\sigma_{Br+/Br}$ as 45.4 Mb in footnote 31, and obtained a branching between the C−Br fission channel and the HBr elimination channel as 55.4:1. When 50.4 Mb is used as the photoionization cross section, the correct C−Br fission:HBr elimination ratio in that system is 49.9:1) The branching ratio between the C−Br bond fission and the HBr elimination channels is given by

$$\frac{\Phi_{Br+CD_2CD_2OH}}{\Phi_{HBr+CD_2CD_2O}} = \frac{\text{integrated signal}_{Br^+}}{\text{integrated signal}_{HBr^+}} \times \frac{\text{expected signal}_{HBr^+}}{\text{expected signal}_{Br^+}} \times \frac{\sigma_{HBr^+/HBr}}{\sigma_{Br^+/Br}}$$
$$= \frac{2.327}{0.01186} \times \frac{1111}{1139} \times \frac{40.0\ \text{Mb}}{50.4\ \text{Mb}}$$
$$= 151.9$$

And the branching ratio between the C−Br bond fission and DBr elimination channels is given by

$$\frac{\Phi_{Br+CD_2CD_2OH}}{\Phi_{DBr+CD_2CDOH}} = \frac{\text{integrated signal}_{Br^+}}{\text{integrated signal}_{DBr^+}} \times \frac{\text{expected signal}_{DBr^+}}{\text{expected signal}_{Br^+}} \times \frac{\sigma_{DBr^+/DBr}}{\sigma_{Br^+/Br}}$$
$$= \frac{2.327}{0.01456} \times \frac{1741}{1037} \times \frac{40.0\ \text{Mb}}{50.4\ \text{Mb}}$$
$$= 212.7$$

The combination of these two ratios yields a total primary photodissociation branching ratio for Br:HBr:DBr as 0.99:0.0064:0.0046. The cofragments formed in the DBr and HBr elimination channels are respectively ethenol, CD_2CDOH (mass = 47) and the CD_2CD_2O (mass = 48) biradical, which may isomerize to acetaldehyde. We detected signal at these mass-to-charge ratios, but because there is also a possible contributing signal from the dissociation channels of the CD_2CD_2OH radical at these mass to charge ratios, this data will be described in the next section.

B. Dissociation Channels of the CD_2CD_2OH Radical. Fitting the signal that results from the unimolecular dissociation of unstable CD_2CD_2OH radicals involves a forward convolution method. A primary $P(E_T)$ characterizes the initial photodissociation, and a forward-convolution fitting method on a guessed $P(E_T)$ for the secondary dissociation of the nascent radicals is used to predict a TOF spectrum. The guessed secondary $P(E_T)$ is iteratively adjusted until a good fit to the data is obtained. An angular distribution of the secondary dissociation of the unstable radicals relative to the initial

dx.doi.org/10.1021/jp212167t | J. Phys. Chem. A XXXX, XXX, XXX−XXX

velocity of the CD_2CD_2OH radical is also a required input parameter. For coplanar dissociations which proceed much slower than the rotational period of the fragment, the daughter fragments are scattered with equal probability in the plane of rotation, and we thus set the angular distribution as $I(\theta) = 1/\sin(\theta)$ in the expression $I(\theta)\sin(\theta)\,d\theta\,d\phi$. Here, z is defined as the direction of the velocity vector of the CD_2CD_2OH radicals prior to dissociation and θ is the angle between that initial velocity vector and the direction of the recoil velocity imparted to the products when the radical dissociates. As $1/\sin(\theta)$ increases to infinity at 0° and 180°, the distribution is leveled off at approximately 9° and 171°, as shown in black solid line in Figure 8 to roughly account for a small out-of-plane

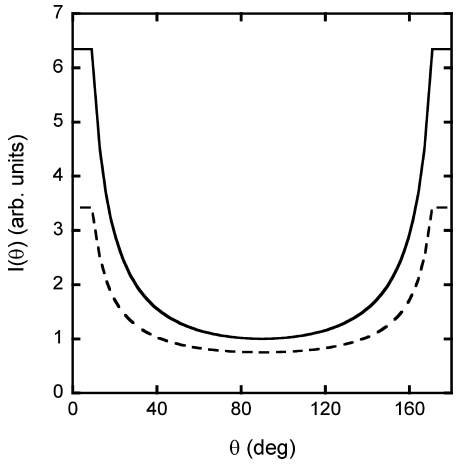

Figure 8. $I(\theta)$ angular distributions used to fit the TOF spectra of secondary dissociations. The angle θ is defined as the angle between the initial velocity vector of the CD_2CD_2OH radical and the direction of recoil imparted during the secondary dissociation. Dissociations which occur on a slower time scale than the rotational period are fit with the $I(\theta) = 1/\sin(\theta)$ distribution shown in solid black line. Those dissociations that proceed on a fast time scale are fit with an angular distribution shown in a dashed line that has a contribution from an isotropic component, so is less strongly peaked along the velocity vector of the dissociating radical.

wobble in the dissociation dynamics. The fits using this angular distribution (which is uniform in θ and ϕ) are highly forward–backward peaked, because of gathering of signal at the poles. For secondary dissociations that take place on a time-scale comparable to the rotational period, we can fit the data by assuming $I(\theta)$ lies somewhere in between $1/\sin(\theta)$ and a constant value. The resulting angular distribution used to fit the data is shown in a dashed line in Figure 8.

In our previous study of the branching of the OH + C_2H_4 reaction,[29] we separately detected the OH (mass = 17) + C_2H_4 (mass = 28) product channel and the CH_3 (mass = 15) + CH_2O (mass = 30) product channel and calculated branching ratios between these channels. In the case of OH + C_2D_4 however, the analogous channels given by eqs 1a and 1c result in products with identical masses; both OH^+ and CD_2H^+ are detected at m/e = 17 and both $C_2D_4^+$ and CD_2O^+ are detected at m/e = 32. We thus must take advantage of the different ionization energies of these species to separately fit each channel. The upper frame of Figure 9 shows the TOF of m/e = 17 fragments taken at 11.27 eV, which lies below the ionization energy of OH^+. All signal taken at this ionization energy must therefore be attributed to CD_2H^+ via eq 1c. The blue solid line

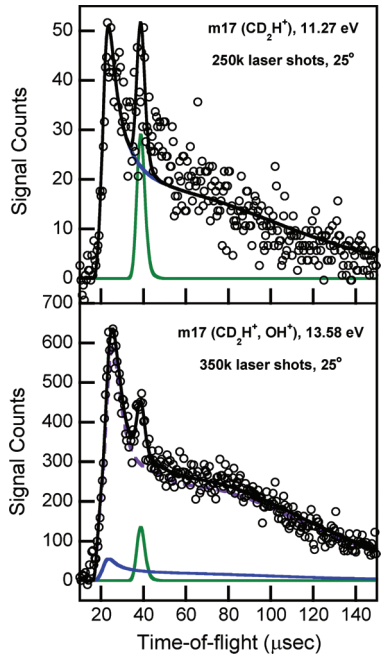

Figure 9. TOF spectra of m/e = 17 fragments taken at a low ionization energy of 11.27 eV (upper frame), to detect the CD_2H products, and 13.58 eV (lower frame) to detect both OH and CD_2H. In both plots, the open circles indicate data, and the green solid line is the fit of the data attributed to the dissociative ionization of stable CD_2CD_2OH radicals to CD_2H^+. The remaining broad signal in the upper frame was attributed to CD_2H formed by the dissociation of unstable CD_2CD_2OH fragments and was fit using the $P(E_T)$ shown in blue solid line in Figure 10 with the angular distribution shown in a dashed line in Figure 8. The majority of the broad signal in the bottom frame was assigned to OH, detected at OH^+ (purple dashed line) from the OH + ethene product channel, though a small portion is fit as CD_2H (blue solid line) from the methyl + formaldehyde channel. The purple fit in the lower frame was derived from the $P(E_T)$ shown in purple dashed line in Figure 10 with the angular distribution shown in solid line in Figure 8.

is the forward convolution fit derived from the blue $P(E_T)$ in Figure 10. The angular distribution shown in dashed line in Figure 8 was used to obtain a good fit to the data. The green solid line is the m/e = 17 signal attributed to the dissociative ionization of stable CD_2CD_2OH radicals, which has an appearance energy (AE) of 10.43 eV.

The lower frame of Figure 9 shows the TOF spectrum of m/e = 17 fragments taken at 13.58 eV, which now has significant contributions from OH^+ via eq 1a. Our study of the OH + C_2H_4 system indicates that the CH_3 + CH_2O channel is quite minor, comprising no more than about 8% of the OH + C_2H_4 product channel.[29] Accordingly, we scale the CD_2H^+ contribution, shown again in blue, to 8% of the total and fit the remaining signal with the angular distribution shown in solid line in Figure 8, attributing it to OH^+. This fit, derived from the purple dashed $P(E_T)$ in Figure 10, is shown in purple dashed line. Additional spectra in the Supporting Information demonstrate that the quality of the fit is relatively insensitive to this scaling factor between the OH^+ and CD_2H^+ fits. No matter how the two contributions are scaled, the $P(E_T)$ for the CD_2CD_2 + OH channel remains peaked at around 8 kcal/mol. Figure 11 shows the TOF spectrum taken at m/e = 32. This signal is attributed to the two cofragments of the m/e = 17 data: $CD_2CD_2^+$ and CD_2O^+. The purple and blue lines are the

dx.doi.org/10.1021/jp212167t | J. Phys. Chem. A XXXX, XXX, XXX–XXX

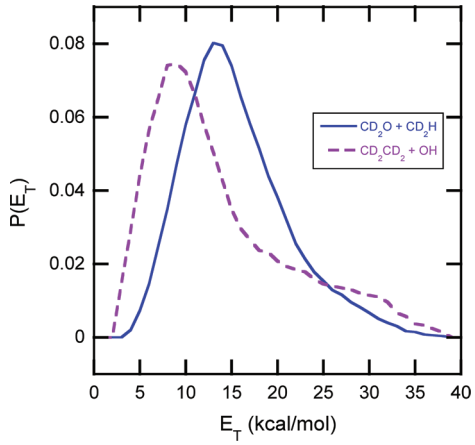

Figure 10. $P(E_T)$'s for the dissociation of unstable CD_2CD_2OH radicals to the CD_2CD_2 + OH and CD_2O + CD_2H pathways are shown in purple dashed and blue solid lines, respectively. These $P(E_T)$'s were obtained by forward convolution fitting of the data in Figure 9. The caption in Figure 11 indicates that the derived $P(E_T)$ is uncertain above 30 kcal/mol.

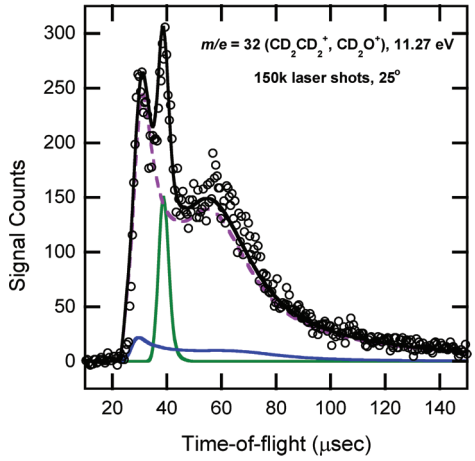

Figure 11. TOF spectrum taken at m/e = 32. The green solid line represents the data attributed to dissociative ionization of stable CD_2CD_2OH radicals. The blue and purple lines represent the fits of data attributed to CD_2O^+ and $CD_2CD_2^+$ respectively, obtained via the forward-convolution of the $P(E_T)$'s in Figure 10, and scaled as in Figure 9. The region near 25 μs is slightly over fit in this plot, and the corresponding 20 μs region in the lower frame of Figure 9 is slightly under fit. The compromise fit in this region results in the derived $P(E_T)$ in Figure 10 being uncertain above 30 kcal/mol.

forward convolution fits from the $P(E_T)$'s of CD_2CD_2 + OH and CD_2O + CD_2H respectively in Figure 10. They have again been scaled to reflect the expected minor branching to the methyl + formaldehyde channel, in accordance with our previous results, but as in the m/e = 17 data, this is only an approximate scaling. The green solid line shows the fit to the data attributed to the dissociative ionization of vibrationally hot stable CD_2CD_2OH radicals (AE = 11.49 eV).

In our prior paper[29] on the dissociation channels of CH_2CH_2OH formed photolytically from 2-bromoethanol, a simple model explains the high recoil kinetic energies imparted to the OH + ethene fragments as the rotationally excited CH_2CH_2OH radical dissociates. The rotational energy of the radical at the transition state en route to OH + ethene is partitioned largely to the relative kinetic energy imparted in this secondary dissociation. Thus, this relative kinetic energy results largely from the tangential velocities of the rotating radical, not from repulsive forces along the OH + ethene reaction coordinate. The other product channels from the highly rotationally excited radicals also show a large partitioning of energy to relative kinetic energy. The bimodal nature of the OH + C_2D_4 $P(E_T)$ can be explained by the fact that the Gg conformer of 2-bromoethanol-d_4 partitions a larger amount of rotational energy to the CD_2CD_2OH fragments (24.4 kcal/mol at E_T = 32 kcal/mol,) than the Tt conformer (13.3 kcal/mol). The highly rotationally excited radicals from the Gg conformer, with correspondingly high tangential velocities, will therefore result in OH and ethene fragments with higher relative kinetic energy than the less rotationally excited radicals from the Tt conformer. Although we estimate that 78% of the parent molecules are in the gauche conformation, the radicals formed from the dissociation of these gauche conformers are more likely to be stable by virtue of the large amount of energy partitioned into rotation. Thus, the unstable radicals that undergo secondary dissociation to OH + ethene are more likely to be formed from the trans conformer, leading to a bimodal $P(E_T)$ whose major peak is the lower translational energy portion. Note that the portion of this $P(E_T)$ above 30 kcal/mol is not well determined by the forward convolution fitting procedure (see figure captions). The fast edges of the OH and C_2D_4 TOF spectra may also both have small contributions from stable CD_2CD_2OH radicals absorbing a second 193 nm photon and dissociating to OH + C_2D_4. Anastasi et al.[56] have estimated the UV absorption cross section of vibrationally thermalized radicals to be 2 × 10^{-18} cm^2·$molecule^{-1}$ at 210 nm, and Karpichev et al.[57] have characterized the excited states of this radical.

Figure 12 shows the data taken at m/e = 30 ($C_2D_3^+$). The green solid line fits the portion of the data attributed to the dissociative ionization of stable CD_2CD_2OH radicals (AE = 9.51 eV), determined from the $P(E_T)$ shown in black dashed line in Figure 3, and the red dashed line fits a contribution from

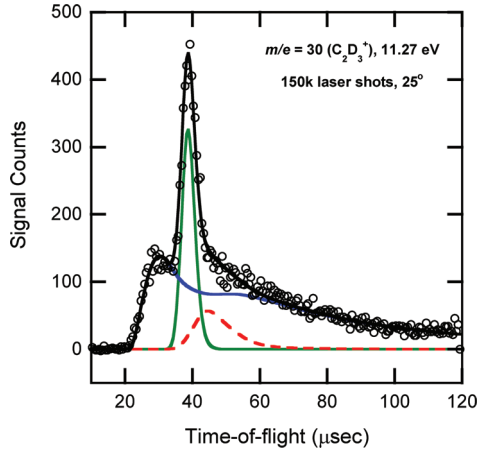

Figure 12. TOF spectrum taken at m/e = 30. The data attributed to dissociative ionization of stable CD_2CD_2OH radicals is shown in green solid line, and the data attributed to the dissociative ionization of the CD_2CDOH cofragment formed in the DBr photoelimination of $BrCD_2CD_2OH$ is shown in a red dashed line. The remaining signal is attributed to $C_2D_3^+$ formed in the secondary dissociation of CD_2CD_2OH radicals. The $P(E_T)$ in Figure 13 is used for the forward-convolution with the angular distribution shown in solid line Figure 8.

dx.doi.org/10.1021/jp212167t | J. Phys. Chem. A XXXX, XXX, XXX–XXX

the dissociative ionization of the CD_2CDOH cofragment formed in the DBr elimination channel (AE = 10.44 eV). The remaining signal was fit in the blue solid line using the $P(E_T)$ shown in Figure 13 for the dissociation of those unstable

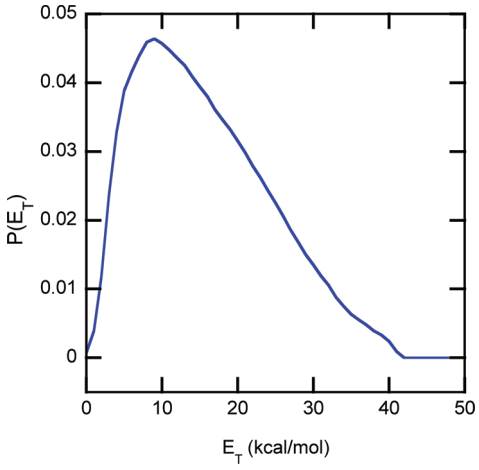

Figure 13. $P(E_T)$ for the dissociation of CD_2CD_2OH radicals to HDO + C_2D_3 derived from the forward-convolution of the m/e = 30 data in Figure 12.

CD_2CD_2OH radicals that form water + vinyl as shown in eq 1b. Although we attempted to collect data at m/e = 19, which we would attribute to the HDO cofragment to C_2D_3, the photoionization cross-section of water was prohibitively low, and thus the signal-to-noise ratio was too poor to definitively fit. The TOF spectrum taken at m/e = 19 is given in the Supporting Information.

In light of the unlikely nature of the water + vinyl reaction pathway, we attempted to find alternative explanations to account for this signal. There are no other products on the PES whose ions would give a mass-to-charge ratio of 30, and so we must consider daughter ions formed upon dissociative ionization, namely, $C_2D_3^+$ from C_2D_4 and CDO^+ from CD_2O. However, several factors make these unlikely sources for the m/e = 30 signal. First, the appearance energies of $C_2D_3^+$ and CDO^+ daughter ions are 13.52 and 12 eV respectively, making them energetically inaccessible at 11.27 eV. Second, the signal intensity in the m/e = 30 data peaks near 150 counts. The signal intensity in the m/e = 32 data attributed to CD_2O^+ peaks at 25 counts for the same number of laser shots. While it is possible that some vibrationally excited CD_2O neutral fragments underwent dissociative ionization despite the high AE, it is unlikely that the daughter ion signal would be present in 6 times the abundance of the parent fragment. Finally, additional plots in the Supporting Information demonstrate that simply attributing all of the data to dissociative ionization of CD_2O yields a poor fit to the data. In addition, one cannot attribute this signal to products formed by the stable radicals potentially absorbing a second 193 nm photon because our vinyl speed distribution was unchanged when the photon flux was reduced by a factor of 10 (see imaging data in Section III.C), and neither transition is saturated.

TOF spectra and photoionization energy (PIE) curves were also taken at m/e = 47 and m/e = 48. Possible sources of this signal include ethenol and acetaldehyde from the dissociation of unstable CD_2CD_2OH radicals (eqs 1d and 1e), the CD_2CD_2O and CD_2CDOH cofragments formed in HBr and DBr elimination pathways, and dissociative ionization of stable CD_2CD_2OH radicals. The poor signal-to-noise, and the similar shape of the various fits in these plots makes definitive assignment of the sources difficult. The plots and detailed analysis are presented in the Supporting Information. In short, we attributed virtually all the m/e = 47 and m/e = 48 data to dissociative ionization of stable CD_2CD_2OH radicals and the CD_2CDOH and CD_2CD_2O cofragments formed in conjunction with DBr and HBr. We approximate that only a very small amount of the signal comes from unstable CD_2CD_2OH radicals dissociating to ethenol or acetaldehyde.

C. Branching Ratios. We now address the theoretical and experimental product branching ratios of the unstable CD_2CD_2OH radicals to the various pathways described in Section III.B and shown in the PES in Figure 1. Our RRKM calculations, summarized in Table 1, predict that the vast

Table 1. Results of the RRKM Predicted and Experimentally Measured Branching Ratios for the Dissociation Pathways of Unstable CD_2CD_2OH Radicals

product channel	RRKM percent branching	experimental branching
OH + C_2D_4	99.95%	80% (combined)
CD_2H + CD_2O	0.0092%	
CD_2CDOH + D	0.0061%	~0%
HDO + C_2D_3	0.039%	20%

majority (99.95%) of unstable radicals with the vibrational energy distribution shown in the lower frame of Figure 1 would dissociate to OH + C_2D_4, but that approximately 0.039% of unstable radicals would dissociate to HDO + C_2D_3, 0.0092% to the CD_2H + CD_2O channel via isomerization to INT 2, and 0.0061% to the CD_2CDOH + D channel via the direct dissociation of unstable INT 1 radicals. (The prediction for the water + vinyl channel was calculated by allowing radicals to access the abstraction transition state, even though the IRC shows this transition state connects the OH + ethene reactants with this product channel, not the radical intermediate.) Our experimental branching ratios are quite different. The overall quantum yield of products from the radicals generated from C−Br photofission in the precursor is given by the following equation:

$$1 = \Phi_{\text{stable radicals}} + \Phi_{C_2D_4+OH} + \Phi_{HDO+C_2D_3} + \Phi_{CD_2H+CD_2O} + \Phi_{\text{acetaldehyde+D/H}} + \Phi_{\text{ethenol+D/H}} \quad (2)$$

$\Phi_{\text{stable radicals}}$ was calculated in this study as 0.8 in Section III.A, which is in close agreement with our studies on the velocity map imaging apparatus,[33] which concluded that 76% of the nascent CD_2CD_2OH radicals were formed stable to subsequent dissociation. Because of the uncertainty in scaling the fits in the m/e = 47 and m/e = 48 signal, as described in the Supporting Information, we cannot accurately measure the fraction of the unstable radicals that dissociate to the acetaldehyde and ethenol pathways. We estimate it to be quite low and take these fractions to be roughly zero. It was calculated in Section III.A that the branching to the DBr and HBr elimination channel comprised less than half a percent of the C−Br fission channel, so we also neglect those photoproducts in this analysis. As we can only get a rough estimate of the partitioning of the m/e = 32 and m/e = 17 data between the OH + C_2D_4 vs CD_2H + CD_2O channels as described in Section III.B, we combine these

dx.doi.org/10.1021/jp212167t | J. Phys. Chem. A XXXX, XXX, XXX−XXX

two sources and instead calculate a branching fraction of the vinyl channel compared to the rest of the available channels:

$$1 = \Phi_{\text{stable}} + \Phi_{\text{HDO}+C_2D_3} + \Phi_{\text{combined } C_2D_4+\text{OH and } CD_2O+CD_2H} \quad (3)$$

The relative signal between the vinyl and the combined m/e = 32 channels was measured by alternately accumulating signal for 50,000 laser shots at m/e = 30 and m/e = 32 three times each, for a total of 150,000 laser shots at each m/e. The branching fraction between the HDO + C_2D_3 channel and the collective C_2D_4 + OH/CD_2H + CD_2O channels was then obtained by integrating the signal counts per laser shot at each m/e and correcting for the 3-D kinematic scattering factors, Jacobian factors, and transit times through the ionizer. The relative signal must also be corrected for the partial photoionization cross sections of each fragment. Assuming that there is virtually no change in photoionization cross section in the deuterated analogues, we take these values to be 8.14 Mb for $C_2D_4^+/C_2D_4$[58] and 22.3 Mb for $C_2D_3^+/C_2D_3$.[59] Though a small portion of the signal at m/e = 32 is likely from formaldehyde, the contribution is minimal so we use the photoionization cross section for ethene here. The total branching ratio is the product of these corrective factors, shown in eq 4. Additional information in the Supporting Information demonstrate that the branching ratio is insensitive to minor adjustments in the percentage of the m/e = 32 signal attributed to C_2D_4.

$$\begin{aligned}\frac{\Phi_{\text{HDO}+C_2D_3}}{\Phi_{\text{OH}+C_2D_4(CD_2H+CD_2O)}} &= \frac{\text{integrated signal}_{m/e=30}}{\text{integrated signal}_{m/e=32}} \times \frac{\text{expected signal}_{C_2D_4}}{\text{expected signal}_{C_2D_3}} \\ &\times \frac{\sigma_{C_2D_4^+/C_2D_4}}{\sigma_{C_2D_3^+/C_2D_3}} \\ &= \frac{0.0469}{0.0644} \times \frac{2596.1}{2763.1} \times \frac{8.14}{22.3} \\ &= 0.25 \end{aligned} \quad (4)$$

Thus, $\Phi_{\text{HDO}+C_2D_3} = 0.25\Phi_{\text{OH}+C_2D_4(CD_2H+CD_2O)}$ and inserting this into eq 3, we obtain the quantum yields $\Phi_{\text{OH}+C_2D_4(CD_2H+CD_2O)} = 0.04$ and $\Phi_{C_2D_4+\text{OH}/CD_2H+CD_2O} = 0.16$. This indicates that 20% of the unstable radicals underwent dissociation to the water + vinyl channel.

This result is in accordance with our previous study,[29] in which we also found the branching to the C_2H_3 + H_2O channel to be much larger than the RRKM predicted branching fraction. The previous work measured the branching fractions of all products, including the formaldehyde + methyl and ethenol/acetaldehyde + H channels, and found that 14.5% of the unstable CH_2CH_2OH radicals underwent dissociation to the water + vinyl channel and that 76.5% of the unstable radicals dissociated to OH + C_2H_4, thus $\Phi_{H_2O+C_2H_3} = 0.19\Phi_{\text{OH}+C_2H_4}$. Even when accounting for the different quantum yield of unstable radicals between the two systems (20% in the deuterated system and 38% in the undeuterated system) the water + vinyl channel is more likely in the deuterated system, relative to the OH + ethene channel, by a factor of 0.20/0.145 = 1.38.

Additional data was taken on a velocity map imaging apparatus to directly measure the quantum yield of the water + vinyl products from the nascent radicals in the deuterated and the undeuterated system. We first determined the quantum yield of the vinyl products from all nascent radicals, both stable and unstable, then corrected it for the different fractions of nascent radicals undergoing dissociation in the two systems. The data was taken using a dual-sample line, in which two bubblers containing $BrCD_2CD_2OH$ and $BrCH_2CH_2OH$ were used to quickly change back and forth between the two parent molecules. Vinyl signal was accumulated in 10,000 laser shot trials, alternating between m/e = 30 ($C_2D_3^+$) and m/e = 27 ($C_2H_3^+$). This ratio of signal intensities must be corrected to account for different number of nascent radicals produced upon irradiation of each precursor with 193 nm light:

$$\frac{\Phi_{\text{HDO}+C_2D_3}}{\Phi_{H_2O+C_2H_3}} = \frac{\text{integrated counts}_{m/e=30}}{\text{integrated counts}_{m/e=27}} \times \frac{\text{C}-\text{Br fission events}_{BrCH_2CH_2OH}}{\text{C}-\text{Br fission events}_{BrCD_2CD_2OH}} \quad (5)$$

A total of 15 trials were taken at m/e = 30 and m/e = 27, for a total of 150,000 laser shots at each mass-to-charge ratio. Figure 14 shows the summed velocity distributions taken in these trials at m/e = 30 ($C_2D_3^+$) and m/e = 27 ($C_2H_3^+$) in the upper and lower frames respectively. The red circles indicate experimental data and the solid lines represent fits to the data using a recently described program[41] designed to derive the secondary

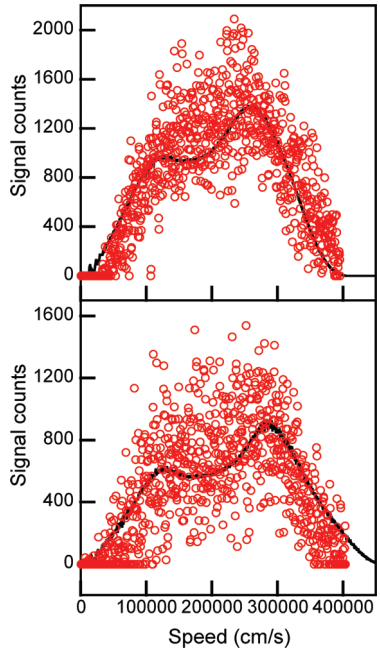

Figure 14. Speed distributions of the products detected at m/e = 30 (upper) and m/e = 27 (lower) using 10.5 eV photoionization in our velocity map imaging apparatus. The red circles are experimental data and the black solid line is a forward-convolution fit to the data. The upper frame shows the C_2D_3 data and was fit using the $P(E_T)$ in Figure 13 and the angular distribution shown in solid line in Figure 8. The lower frame shows the C_2H_3 data from the dissociation of 2-bromoethanol, and was fit using the analogous $P(E_T)$ in Figure 18 of ref 29 and the angular distribution shown in solid line in Figure 8. The unfit signal is due to dissociative ionization of stable radicals. The signal at low speeds is reduced to a burn spot near the center of the chevron detector, and a small fraction of the fragments at highest net speeds plotted went beyond the active region of the detector.

dx.doi.org/10.1021/jp212167t | J. Phys. Chem. A XXXX, XXX, XXX−XXX

dissociation $P(E_T)$, given a certain 1° $P(E_T)$, from a forward convolution fit to the measured net velocity distribution. The forward-convolution fitting method, described in more detail in ref 41, uses the $P(E_T)$'s of unstable CD_2CD_2OH and CH_2CH_2OH radicals obtained on the velocity map imaging apparatus in our previous papers[29,33] to characterize the primary dissociation of the parent molecule in each system. A guessed $P(E_T)$ for the secondary dissociation is used to predict the velocity distribution of vinyl products that would result from this $P(E_T)$. For the deuterated system, the secondary $P(E_T)$ used to fit the NSRRC vinyl data shown in Figure 13 was used to obtain the solid line fit in the upper frame of Figure 14. For the undeuterated system, the corresponding fit to the NSRRC data from ref 29 was used to obtain the fit in the lower frame of Figure 14. Additional plots in the Supporting Information show upper and lower bounds to the scaled fits. The relative signal intensity is obtained by integrating the fits in both spectra to yield $(298 \pm 50) \times 10^6$ counts of $m/e = 30$ signal, and $(209 \pm 45) \times 10^6$ counts of $m/e = 27$ signal. The margins of error were derived by integrating the area below the upper and lower bounds to the fit.

We note here that both plots, while fairly well fit on the fast and slow sides, are under-fit in the 1500−2500 m/s region. This is because a portion of the $m/e = 30$ or $m/e = 27$ signal is from the dissociative ionization of stable CD_2CD_2OH or CH_2CH_2OH radicals, as described in Section III.B. The over fitting in the <500 m/s region of both spectra is likely due to the small region of dead pixels near the center of our imaging detector. We attribute the over fitting in the >4000 m/s region of the $m/e = 27$ spectrum to fragments lost at the outer edge of the detector. Our current apparatus parameters permit the detection of fragments with velocities up to 4000 m/s with the ion optic voltages used. The smaller $m/e = 27$ fragments have a small percentage with velocities higher than this, while the heavier $m/e = 30$ fragments do not. Nevertheless, the agreement between the NSRRC vinyl data taken at an ionization energy of 11.27 eV and the velocity map imaging vinyl data taken at 10.5 eV serves as an indication that the signal is from vinyl, not from the dissociative ionization of C_2D_4 or CD_2O. Indeed, the appearance energy of $C_2D_3^+$ from ethene and CDO^+ from formaldehyde is much higher than 10.5 eV.

The relative number of C−Br fission events in each system is determined by measuring the signal between $Br(^2P_{1/2})$ formed from the dissociation of $BrCD_2CD_2OH$ and from the dissociation of $BrCH_2CH_2OH$. The relative bromine signal is indicative of slightly different vapor pressures and absorption cross sections of the two parent molecules. Signal was accumulated in 60,000 laser shot trials, alternating between the two samples for a total of 5 trials. The ratio of integrated signal counts for the undeuterated system to the deuterated system was found to be 0.562 ± 0.05, and when corrected for the ratio of previously determined spin−orbit branching ratios to account for both excited and ground spin−orbit states, the relative number of dissociation events is equal to 0.537 ± 0.18.

The relative branching to the vinyl channel in each system is thus given by inserting the measured quantities into eq 5, yielding:

$$\frac{\Phi_{HDO+C_2D_3}}{\Phi_{H_2O+C_2H_3}} = \frac{(298 \pm 50) \times 10^6}{(209 \pm 45) \times 10^6} \times 0.537 \pm 0.092 = 0.766 \pm 0.25 \quad (6)$$

This value of 0.766 would indicate that the branching to the water + vinyl channel is diminished by the substitution of hydrogen with deuterium. This is the result we might expect if tunneling were responsible for such a high prevalence of this channel. However, we determined in our previous paper[33] that a large percentage of the CD_2CD_2OH radicals were formed stable to further dissociation. By scaling the $P(E_T)$ derived from the velocity distribution of CD_2CD_2OH radicals to that derived from the velocity distribution of Br atoms, we determined that nearly 80% of nascent radicals were stable. The analogous number for the undeuterated system is 63%. However, both these numbers are dependent on the scaling of the two $P(E_T)$'s. Thus the yield of vinyl products from the radicals that did dissociate is larger for the partially deuterated system, not smaller. Multiplying 0.766 by 0.38/0.23, to account for the differing fraction of unstable radicals in the two systems as measured from the imaging data, gives 1.27. Although it is an approximate value, it is in good agreement with the value of 1.38 obtained from the NSRRC data above.

IV. DISCUSSION

This paper describes our recent efforts to characterize the product pathways in the OH + ethene reaction by selectively replacing hydrogen with deuterium in ethene. Using the $BrCD_2CD_2OH$ precursor, we first characterized two minor photodissociation channels that were previously indistinguishable: the two competing hydrogen bromide photoelimination pathways. We then investigated the dissociation dynamics of the CD_2CD_2OH radicals from the major C−Br photofission channel to further characterize an interesting product channel observed in our prior work,[29] the dissociation of this radical to water + vinyl. We had attributed these products to a frustrated dissociation toward OH + ethene followed by H-atom abstraction by the OH moiety, and we find in this work that a larger than predicted percentage of stable radicals is also undergoing dissociation to HDO + C_2D_3. In our previous paper,[33] we characterized the range of vibrational energies partitioned to the CD_2CD_2OH radicals by the photodissociation of the $BrCD_2CD_2OH$ parent molecule. We have now determined that of the unstable CD_2CD_2OH radicals formed, 20% of these will dissociate to the HDO + C_2D_3 channel, with the remaining 80% dissociating to either OH+ C_2D_4 or CD_2H + CD_2O, and a very small amount dissociating to CD_2CDOD + H.

The results in this paper provide valuable information about the dynamics of the water + vinyl channel. The experimentally determined branching to this channel, much higher than the statistical transition state calculations, indicates that the dynamics governing this reaction are unlike that governing the other pathways. It is well understood that dissociation channels like that to OH + ethene do not have a good dividing surface in a statistical transition state prediction, and so require a variational correction. However it has been traditional to assume that the flux that does not make it all the way to the OH + ethene product asymptote simply returns to the CH_2CH_2OH radical reactant well. In our prior paper on the OH + C_2H_4 system, we proposed that the large branching to the water + vinyl channel might result if these frustrated dissociation trajectories underwent an H-atom abstraction process en route back to the CH_2CH_2OH well. This process is similarly described as a roaming pathway, identified in the classical trajectory calculations of Kamarchik et al.[30] However in our prior paper we noted that the classical trajectories only

dx.doi.org/10.1021/jp212167t | J. Phys. Chem. A XXXX, XXX, XXX−XXX

evidenced a few percent branching to this product channel from radicals with 44 kcal/mol of total energy relative to the zero point level of CH_2CH_2OH, with microcanonical sampling. We put forth the possibility that we observed a larger branching to the H_2O + vinyl channel than the theoretical prediction because tunneling might be important in the dynamics. Thus we initiated the present study to test this idea, as abstraction of a D atom by the OH moiety would be expected to be less probable if much of the product flux required tunneling through the abstraction barrier. Our experimental results, discussed below, suggest that tunneling does not play a major role in the observed branching fraction to the water + vinyl product channel in these systems. Rather, the branching ratio between OH + ethene and water + vinyl might instead be sensitive to the high angular momentum of the β-hydroxyethyl radicals studied in these experiments, because the moment of inertia at the transition state for the abstraction reaction is larger than that at the OH + ethene bottleneck.

The dissociation pathway of β-hydroxyethyl radicals to water + vinyl involves H-atom motion in the undeuterated system, and D-atom motion in the deuterated system. If tunneling through these barriers was a significant factor in this dissociation pathway, the branching to the water + vinyl pathway would be decreased upon deuteration, as the tunneling would then involve D-atom motion to form HDO. However, our experimental results did not show a decrease in branching to the water + vinyl channel upon this deuteration. Instead, the branching increased slightly when we corrected for the differing fraction of stable radicals in the two systems. This result is not dependent on the different viewing times inherent in the branching fraction measurements on the two apparatuses. We note that the two apparatuses described in this paper differ significantly in the length of time between the generation of the nascent radicals and the time window in which they must dissociate for the products of that dissociation to be detected. In the crossed laser-molecular beam apparatus, the neutral radicals must dissociate in less than 5 microseconds for the products to be born within the viewing angle of the detector aperture, whereas in the velocity map imaging apparatus, only products produced in the 40 ± 10 ns between the photodissociation and photoionization lasers will be detected. If tunneling was quite slow but still contributed a significant fraction to the water + vinyl dissociation pathway for our population of nascent radicals, then we might be sensitive to this channel in the scattering data but not in the imaging data. However the measurements of the relative branching to this product channel were in good agreement between the two apparatuses, so the different viewing times inherent in each measurement are not substantially affecting the measured branching ratios.

We now consider another possibility for the unexpectedly large branching to the water + vinyl dissociation channel that is not dependent upon quantum tunneling. In the classical trajectory calculations of Kamarchik et al.,[30] which predicted only a small branching to this channel even at 44 kcal/mol relative to the zero point level of the β-hydroxyethyl radical, the radicals were not highly rotationally excited. In contrast, we generated highly rotationally excited radicals in this experimental study. The $P(E_{int})$ of these radicals is shown in a red dashed line in the upper frame of Figure 1. As part of our previous analysis,[33] we modeled the rotational energy imparted to the radicals as $E_{rot} = (\mu b^2/I)E_T$, where μ is the reduced mass of the Br + CD_2CD_2OH system, b is the impact parameter, and I is the moment of inertia of the CD_2CD_2OH radical moiety. We subtracted the rotational energy from the total internal energy to yield the $P(E_{vib})$ of the radicals shown in red in the lower frame of Figure 1. While this $P(E_{vib})$ was quite useful in aiding our understanding of the experimental $P(E_T)$ for the portion of dissociation events that resulted in stable radicals, the rotational energy of the β-hydroxyethyl radical plays a critical role in the dynamics of its dissociation and should not be neglected here. It is important to consider the change in the moment of inertia of the β-hydroxyethyl radical as is dissociates to either OH + ethene, or undergoes the H- or D-abstraction pathway to form water + vinyl.

In our previous paper, we calculated via a modified impulsive model that C−Br bond fission imparts a large amount of recoil kinetic energy to the Br and CD_2CD_2OH fragments, and that the impulsive force is off-axis from the center of mass of the radical. Thus, the radical is generated with high angular momentum and has correspondingly high rotational energy about an axis perpendicular to the plane defined by the center-of-mass of the nascent radical and the impulsive force along the C−Br bond.[32,33] We calculated the moment of inertia about the axis of the CD_2CD_2OH radical moiety as 60.7 amu·Å^2 from the Gg conformer (the corresponding value for an impulsive dissociation from the Tt conformer is 64.6 amu·Å^2).[33] Using the C1 transition state of Senosiain et al. (with appropriate D/H substitution) we calculate that the transition state of the OH + C_2D_4 dissociation pathway has a moment of inertia about this same axis of rotation of 65.3 amu·Å^2 from the Gg conformer (83.1 from the Tt conformer) and the transition state of the D-abstraction pathway to HDO + C_2D_3 has a moment of inertia of 113.0 amu·Å^2 from the Gg conformer (119.1 from the Tt conformer). Because angular momentum is conserved, as a dissociative trajectory nears the abstraction transition state with its larger moment of inertia than the bottleneck in the dissociation to OH + ethene, a larger fraction of the rotational energy in the nascent radicals is converted to vibrational energy and made available to surmount the abstraction barrier. From this we conclude that the increased branching to the water + vinyl channel of highly rotationally excited β-hydroxyethyl radicals may be because the dynamics on the potential energy surface is substantially influenced by centrifugal terms.

To characterize how the high angular momentum of the radical might affect the branching between the OH + ethene and water + vinyl channels, we calculated an approximate centrifugal correction for the energies along the reaction coordinates of these dissociation pathways. Figure 15 shows two sets of intrinsic reaction coordinates (IRCs), calculated at the B3LYP/6-311+G(2df,p) level of theory, and scaled to the zero-point corrected G4 energies in Figure 1. The lower traces, denoted by circles, follow the pathway between the β-hydroxyethyl radical and OH + ethene. The upper traces denoted by diamonds follow the D-atom abstraction pathway between OH + ethene and the transition state for the HDO + C_2D_3 abstraction channel. The lower and upper x-axes denote the reaction coordinate of the OH + ethene addition pathway and the D-atom abstraction pathway, respectively. The two traces are aligned such that the C−O bond lengths in each trace both have a value of 2.95 Å at $x_{lower} = 0$ and $x_{upper} = 5$. The black curves show the uncorrected and scaled B3LYP/6-311+G(2df,p) energies from the IRC calculation. It is clear here that when no correction is made, the transition state for the D-atom abstraction pathway lies 6 kcal/mol higher than the

dx.doi.org/10.1021/jp212167t | J. Phys. Chem. A XXXX, XXX, XXX−XXX

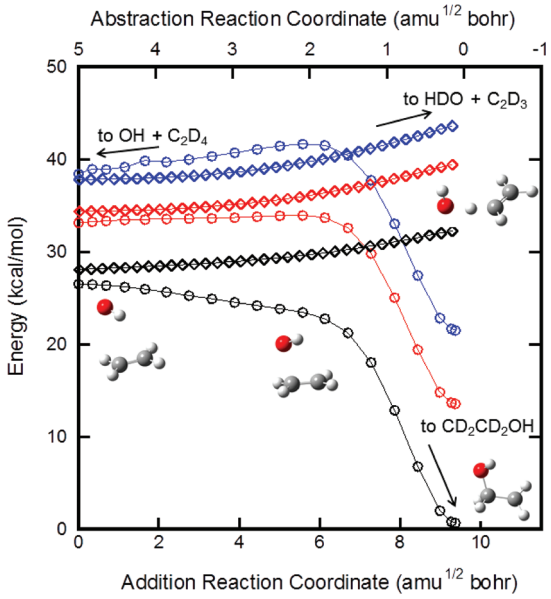

Figure 15. Uncorrected and centrifugally corrected IRCs for two pathways on the OH + ethene PES. The three lower curves, denoted by circle markers, trace the pathway from the CD_2CD_2OH radical to OH + ethene. The reaction coordinate for these traces is denoted on the lower *x*-axis. The three uphill curves, denoted by diamond markers, trace the abstraction pathway from OH + ethene to the TS leading to water + vinyl. The reaction coordinate for these curves is denoted on the upper *x*-axis. The black curves in each set denote uncorrected energies from the IRC calculation scaled to the zero point corrected G4 energies in Figure.1. The red and blue curves represent the centrifugally corrected energies of radicals generated by the Tt and Gg conformers of 2-bromoethanol-d_4, respectively. The diagrams at the edges of the plot indicate the geometry of the radical at the stationary points on the IRC. The geometry in the middle is the structure at the maximum of the centrifugally corrected energies of the IRC for the Gg conformer. It is only 2 kcal/mol lower than the centrifugally corrected energy for the abstraction transition state.

transition state for the direct dissociation of β-hydroxyethyl radicals to OH + ethene.

The moments of inertia about the initial axis of rotation were then calculated for many geometries along these two IRCs. At each geometry, a centrifugal correction given by $E_{corr} = (\mu b^2/I')E_T$ was added to the B3LYP energy generated by the IRC calculation. Here, I' is the moment of inertia at the geometry of interest, μ (30.37 amu) and b (0.93 Å for the Tt conformer, and 1.23 Å for the Gg conformer) remain unchanged from the photodissociation of the parent molecule. The centrifugal corrections were made for radicals generated from both the Tt and the Gg conformers of 2-bromoethanol-d_4. The Gg conformer imparts much more rotational energy to the β-hydroxyethyl radicals, because of its higher value of b and lower value of I, and this allows us to examine how the PES changes at a low and a high value of J. The corrections were calculated using the average value of E_T for the unstable radicals, 32 kcal/mol for the Tt conformer and 29 kcal/mol for the Gg conformer.

The resulting centrifugally corrected energies along these two reaction coordinates are shown in red (Tt conformer) and blue (Gg conformer) in Figure 15. The centrifugal correction results in a fairly uniform change to the D-atom abstraction pathway. However, the correction has a pronounced effect on the shape of the PES on the pathway connecting the radical to the OH + ethene exit channel. The effective transition state, given by the maximum along the corrected PES, shifts closer to the geometry of the radical. Additionally, as more rotational excitation is introduced to the radicals, the energy difference between the effective transition states of the two pathways decreases, and the exit channel become distinctly less flat and more downhill. Because the energy difference between the two transition states has decreased with these centrifugal corrections, to 5.5 kcal/mol for radicals from the Tt conformer and only 2 kcal/mol for the radicals from the Gg conformer, one might expect a more substantial branching to HDO + C_2D_3 than for a rotationally cold radical. To work toward a more accurate prediction for the branching to the HDO + C_2D_3 products, one would want to account for centrifugal effects on the dynamics on the global potential energy surface; merely correcting the energies along the $J = 0$ reaction coordinate as done here gives only qualitative insight. It would be very interesting to see if the classical trajectory calculations on the global potential energy surface predicted a larger branching to the water + vinyl product channel if microcanonical sampling of the nascent radicals included a high angular momentum about the axis defined by the impulsive dissociation of the precursor in our experiments.

■ ASSOCIATED CONTENT

Supporting Information

Additional TOF spectra and fits, number density of the molecular beam velocity distribution, secondary $P(E_T)$ comparisons from the deuterated and undeuterated system, and tables of calculated appearance energies. This material is available free of charge via the Internet at http://pubs.acs.org.

■ AUTHOR INFORMATION

Corresponding Author

*E-mail: L-Butler@uchicago.edu.

Notes

The authors declare no competing financial interest.

■ ACKNOWLEDGMENTS

This work was supported by the Chemical Sciences, Geosciences and Biosciences Division, Office of Basic Energy Sciences, Office of Science, U.S. Department of Energy, under Grant DE-FG02-92ER14305 (L.J.B.). Synchrotron beam time and additional funding were provided by the National Synchrotron Radiation Research Center and Academica Sinica. We gratefully acknowledge the invaluable help at the NSRRC by Wen-Jian Huang, Yi-Cheng Lin, Chen-Hsun Tsai, and Andrew F. Chen. We would also like to thank Dr. Chow-Shing Lam for assistance in the IRC calculations. Finally, we would very much like to thank "Ravi", the father of atmospheric chemistry at NOAA, for encouraging our work on the chemistry of radical intermediates.

■ REFERENCES

(1) Tully, F. P. *Chem. Phys. Lett.* **1988**, *143*, 510−514.
(2) Vakhtin, A. B.; Murphy, J. E.; Leone, S. R. *J. Phys. Chem. A* **2003**, *107*, 10055−10062.
(3) Bradley, J. N.; Capey, W. D.; Fair, R. W.; Pritchard, D. K. *Int. J. Chem. Kinet.* **1976**, *8*, 549−561.
(4) Tully, F. P. *Chem. Phys. Lett.* **1983**, *96*, 148−153.
(5) Morris, E. D.; Stedman, D. H.; Niki, H. *J. Am. Chem. Soc.* **1971**, *93*, 3570−3572.

(6) Cool, T. A.; Nakajima, K.; Mostefaoui, T. A.; Qi, F.; McIlroy, A.; Westmoreland, P. R.; Law, M. E.; Poisson, L.; Peterka, D. S.; Ahmed, M. *J. Chem. Phys.* **2003**, *119*, 8356−8365.
(7) Taatjes, C. A.; Hansen, N.; McIlroy, A.; Miller, J. A.; Senosiain, J. P.; Klippenstein, S. J.; Qi, F.; Sheng, L.; Zhang, Y.; Cool, T. A.; Wang, J.; Westmoreland, P. R.; Law, M. E.; Kasper, T.; Kohse-Höinghaus, K. *Science* **2005**, *308*, 1887−1889.
(8) Taatjes, C. A.; Hansen, N.; Miller, J. A.; Cool, T. A.; Wang, J.; Westmoreland, P. R.; Law, M. E.; Kasper, T.; Kohse-Höinghaus, K. *J. Phys. Chem. A* **2005**, *110*, 3254−3260.
(9) Bradley, J. N.; Hack, W.; Hoyermann, K.; Wagner, H. G. *J. Chem. Soc., Faraday Trans. I* **1973**, *69*, 1889−1898.
(10) Smith, I. W. M.; Zellner, R. *J. Chem. Soc., Faraday Trans II* **1973**, *69*, 1617−1627.
(11) Farquharson, G.; Smith, R. *Aust. J. Chem.* **1980**, *33*, 1425−1435.
(12) Atkinson, R.; Aschmann, S. M.; Winer, A. M.; Pitts, J. N. *Int. J. Chem. Kinet.* **1982**, *14*, 507−516.
(13) Atkinson, R.; Aschmann, S. M. *Int. J. Chem. Kinet.* **1984**, *16*, 1175−1186.
(14) Liu, A.-D.; Mulac, W. A.; Jonah, C. D. *Int. J. Chem. Kinet.* **1987**, *19*, 25−34.
(15) Liu, A.; Mulac, W. A.; Jonah, C. D. *J. Phys. Chem.* **1988**, *92*, 3828−3833.
(16) Bott, J. F.; Cohen, N. *Int. J. Chem. Kinet.* **1991**, *23*, 1075−1094.
(17) Becker, K. H.; Geiger, H.; Weisen, P. *Chem. Phys. Lett.* **1991**, *184*, 256−261.
(18) Klein, T.; Barnes, I.; Becker, K. H.; Fink, E. H.; Zabel, F. *J. Phys. Chem.* **1984**, *88*, 5020−5025.
(19) Kuo, C. H.; Lee, Y. P. *J. Phys. Chem.* **1991**, *95*, 1253−1257.
(20) Diau, E. W.-G.; Lee, Y.-P. *J. Chem. Phys.* **1992**, *96*, 377−386.
(21) Chuong, B.; Stevens, P. S. *J. Phys. Chem. A* **2000**, *104*, 5230−5237.
(22) Hippler, H.; Viskolcz, B. *Phys. Chem. Chem. Phys.* **2000**, *2*, 3591−3596.
(23) Senosiain, J. P.; Klippenstein, S. J.; Miller, J. A. *J. Phys. Chem. A* **2006**, *110*, 6960−6970.
(24) Zhu, R. S.; Park, J.; Lin, M. C. *Chem. Phys. Lett.* **2005**, *408*, 25−30.
(25) Sosa, C.; Schlegel, H. B. *J. Am. Chem. Soc.* **1987**, *109*, 7007−7015.
(26) Sosa, C.; Schlegel, H. B. *J. Am. Chem. Soc.* **1987**, *109*, 4193−4198.
(27) Yamada, T.; Bozzelli, J. W.; Lay, T. *J. Phys. Chem. A* **1999**, *103*, 7646−7655.
(28) Srinivasan, N. K.; Su, M. C.; Michael, J. V. *Phys. Chem. Chem. Phys.* **2007**, *9*, 4155−4163.
(29) Ratliff, B. J.; Alligood, B. W.; Butler, L. J.; Lee, S.-H.; Lin, J. J.-M. *J. Phys. Chem. A* **2011**, *115*, 9097−9110.
(30) Kamarchik, E.; Koziol, L.; Reisler, H.; Bowman, J. M.; Krylov, A. I. *J. Phys. Chem. Lett.* **2010**, *1*, 3058−3065.
(31) Hintsa, E. J.; Zhao, X.; Lee, Y. T. *J. Chem. Phys.* **1990**, *92*, 2280−2286.
(32) Ratliff, B. J.; Womack, C. C.; Tang, X. N.; Landau, W. M.; Butler, L. J.; Szpunar, D. E. *J. Phys. Chem. A* **2010**, *114*, 4934−4945.
(33) Womack, C. C.; Booth, R. S.; Brynteson, M. D.; Butler, L. J.; Szpunar, D. E. *J. Phys. Chem. A* **2011**, *115*, 14559−14569.
(34) Edwards, L. W.; Ryazanov, M.; Reisler, H.; Klippenstein, S. J. *J. Phys. Chem. A* **2010**, *114*, 5453−5461.
(35) Lin, J. J.; Chen, Y.; Lee, Y. Y.; Lee, Y. T.; Yang, X. *Chem. Phys. Lett.* **2002**, *361*, 374−382.
(36) Lee, S.-H.; Lee, Y.-Y.; Lee, Y. T.; Yang, X. *J. Chem. Phys.* **2003**, *119*, 827−838.
(37) Wang, C. C.; Lee, Y. T.; Lin, J. J.; Shu, J.; Lee, Y.-Y.; Yang, X. *J. Chem. Phys.* **2002**, *117*, 153−160.
(38) FitzPatrick, B. L.; Alligood, B. W.; Butler, L. J.; Lee, S.-H.; Lin, J. J.-M. *J. Chem. Phys.* **2010**, *133*, 094306−094321.
(39) Eppink, A. T. J. B.; Parker, D. H. *Rev. Sci. Instrum.* **1997**, *68*, 3477−3484.
(40) Parker, D. H.; Eppink, A. T. J. B. *J. Chem. Phys.* **1997**, *107*, 2357−2362.
(41) Alligood, B. W.; Straus, D. B.; Butler, L. J. *J. Chem. Phys.* **2011**, *135*, 034302−034308.
(42) Alligood, B. W.; Womack, C. C.; Brynteson, M. D.; Butler, L. J. *Int. J. Mass Spectrom.* **2011**, *304*, 45−50.
(43) Chang, B.-Y.; Hoetzlein, R. C.; Mueller, J. A.; Geiser, J. D.; Houston, P. L. *Rev. Sci. Instrum.* **1998**, *69*, 1665−1670.
(44) Dribinski, V.; Ossadtchi, A.; Mandelshtam, V. A.; Reisler, H. *Rev. Sci. Instrum.* **2002**, *73*, 2634−2642.
(45) Frisch, M. J.; Trucks, G. W.; Schlegel, H. B.et al. *Gaussian 09*, Revision A.02; Gaussian, Inc.: Wallingford, CT, 2009.
(46) Baker, J. R.; Ortiz, N. F.; Preses, J. M.; Lohr, L. L.; Maranzana, A.; Stimac, P. J., Nguyen, T. L.; Kumar, T. J. D. *MultiWell-2011.1 Software*; University of Michigan: Ann Arbor, MI, 2011; http://aoss.engin.umich.edu/multiwell/.
(47) Barker, J. R. *Int. J. Chem. Kinet.* **2001**, *33*, 232−245.
(48) Barker, J. R. *Int. J. Chem. Kinet.* **2009**, *41*, 748−763.
(49) Scott, A. P.; Radom, L. *J. Phys. Chem.* **1996**, *100*, 16502−16513.
(50) Butler, L. J.; Hintsa, E. J.; Shane, S. F.; Lee, Y. T. *J. Chem. Phys.* **1987**, *86*, 2051−2074.
(51) Escure, C.; Leininger, T.; Lepetit, B. *J. Chem. Phys.* **2009**, *130*, 244305−244310.
(52) Lin, D.; Saha, H. P. *Phys. Rev. A* **1999**, *59*, 3614−3621.
(53) Miller, J. L.; Krisch, M. J.; Butler, L. J.; Shu, J. *J. Phys. Chem. A* **2005**, *109*, 4038−4048.
(54) Morton, M. L.; Miller, J. L.; Butler, L. J.; Qi, F. *J. Phys. Chem. A* **2002**, *106*, 10831−10842.
(55) Gallagher, J. W.; Brion, C. E.; Samson, J. A. R.; Langhoff, P. W. *J. Phys. Chem. Ref. Data* **1988**, *17*, 9−153.
(56) Anastasi, C.; Simpson, V.; Munk, J.; Pagsberg, P. *J. Phys. Chem.* **1990**, *94*, 6327−6331.
(57) Karpichev, B.; Koziol, L.; Diri, K.; Reisler, H.; Krylov, A. I. *J. Chem. Phys.* **2010**, *132*, 114308−114308.
(58) Cool, T. A.; Wang, J.; Nakajima, K.; Taatjes, C. A.; McLlroy, A. *Int. J. Mass Spectrom.* **2005**, *247*, 18−27.
(59) Taatjes, C. A., Private Communication, 2008.